12th International Symposium on Turbulence and Shear Flow Phenomena (TSFP12)
Osaka, Japan (Online), July 19-22, 2022

# A COMPARISON OF SPATIAL AND TEMPORAL ACCELERATION IN TURBULENT CHANNEL FLOWS

**Matthew A. Falcone**
Department of Mechanical Engineering
University of Sheffield
Sir Frederick Mappin Building, Mappin Street, Sheffield, S1 3JD, UK
mfalcone1@sheffield.ac.uk

**Shuisheng He**
Department of Mechanical Engineering
University of Sheffield
Sir Frederick Mappin Building, Mappin Street, Sheffield, S1 3JD, UK
s.he@sheffield.ac.uk

## ABSTRACT

A direct comparison of a temporal and an idealised spatial acceleration incorporating moving walls has been performed using Direct Numerical Simulation by equating the bulk flow inertia of the two cases, which resulted in both flows having the same bulk velocity when a convective distance was defined. It was found that the key features of the two flows were similar and conformed to the transition theory proposed by He & Seddighi (2013) for temporal acceleration. However, a number of differences were found. These include the response of the skin friction coefficient, the initial increase of which was significantly reduced in the moving-wall acceleration, and the location of transition, which occurred significantly earlier in the moving wall case. A novel pseudo-body force approach has been developed to understand the differences in the flow evolution in the moving wall and temporal accelerations.

## INTRODUCTION

Spatially and temporally accelerating flows are present in a range of engineering applications. This results in a need for an in-depth understanding of these flows, which can include complex and not well-understood phenomena, including laminarisation. Temporally developing flows have long been used in the study of spatially developing flows, including in transition (Wray & Hussaini, 1984), developing turbulent boundary layers (Kozul *et al.*, 2016), and three-dimensional boundary layers (Coleman *et al.*, 1996). Spatial and temporal accelerations contain a number of overarching similarities, such as the initial freezing of the Reynolds stresses. In this context, we can consider the extent to which temporally accelerating flows can be used to understand their spatial counterparts.

Significant developments have been made over the past few years in the understanding of temporal acceleration (He & Seddighi, 2013; Sundstrom & Cervantes, 2018; Guerrero *et al.*, 2021), which have found that the flow development can be characterised by the development of a new boundary layer superimposed on the pre-existing flow. Initially, the new boundary layer does not significantly alter the flow characteristics, although it modulates the pre-existing turbulence structures. Eventually, the flow undergoes a spontaneous transition, in a process resembling bypass transition. Recently, we have carried out a study of spatially accelerating flow incorporating moving walls to investigate the effect of flow acceleration without the streamline contraction intrinsic to a more conventional spatial acceleration (Falcone & He, 2022). This moving-wall flow has been found to exhibit very similar phenomena to that observed in temporal acceleration. It was found that this flow could similarly be understood in terms of the theory developed in He & Seddighi (2013). In this paper, we directly compare the temporal and moving wall accelerations to understand the similarities and differences in the transition processes of each flow.

## METHODOLOGY

Direct Numerical Simulations of turbulent channel flow have been performed using the solver CHAPSim (He & Seddighi, 2013; Seddighi-Moormani, 2011). The spatial acceleration has been implemented by applying a streamwise decreasing velocity on the channel walls. In this case, a linear acceleration profile has been used such that the wall velocity, $U_w = -Cx$, where $x$ is the distance from the onset of the acceleration and $C$ is a positive constant. This results in a relative acceleration between the fluid and the wall with the relative bulk velocity defined as $U_b = U_0 - U_w = U_0 + Cx$. This is depicted in figure 1. The temporal acceleration has been imposed by applying a uniform body force. In order to compare the temporal and spatial accelerations, the bulk temporal inertia, $dU_b/dt$ (for the temporal acceleration) and the spatial inertia of the bulk flow, $U_b dU_b/dx$ (for the moving-wall acceleration) were equated. Given the linear relative bulk velocity profile for the moving-wall acceleration, the bulk velocity in the temporal acceleration can be obtained from the following differential equation.

$$\frac{dU_b(t)}{dt} = U_b \frac{dU_b}{dx} = CU_b \tag{1}$$

Table 1. Case setup for the moving-wall and temporal accelerations

| | $Re_0$ | $Re_1$ | $\Delta x_{conv}$ | Domain ($X \times Y \times Z$) | Mesh ($X \times Y \times Z$) | $\Delta x^+_{max}$ | $\Delta y^+_{w,max}$ | $\Delta y^+_{c,max}$ | $\Delta z^+_{max}$ |
|---|---|---|---|---|---|---|---|---|---|
| Case M | 2800 | 4237 | 15 | $30 \times 2 \times 4$ | $1296 \times 256 \times 270$ | 5.9 | 0.3 | 3.3 | 3.8 |
| Case T | 2800 | 7840 | $\sim 50$ | $18 \times 2 \times 5$ | $1000 \times 324 \times 480$ | 7.7 | 0.4 | 4.3 | 4.5 |

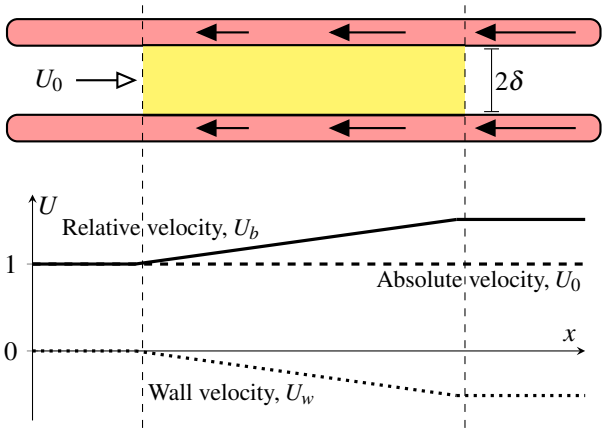


Figure 1. Flow acceleration caused using the moving-wall approach. Top: The channel and its streamwise boundary condition are shown with the filled black arrows representing the wall velocity. The shaded yellow region is the region where the acceleration is applied. Bottom: A plot showing the variation of the absolute velocity (dashed), wall velocity (dotted), and relative velocity (solid).

The resulting bulk velocity for the temporal acceleration is

$$U_b(t) = U_{b0}\exp(Ct). \tag{2}$$

To compare the two flows, a convective distance can be defined, $x_{conv}$ which considers the distance travelled by a fluid particle moving at the bulk velocity.

$$x_{conv}(t) = \int_0^t U_b(\tau)d\tau \tag{3}$$

For equation 2, the convective distance is given by $x_{conv} = U_b(t)/C$, which shows that the bulk velocity in the temporal case varies linearly with its convective distance and hence shows that the two flows are equivalent in the bulk sense. It can also be shown that the values of acceleration parameter, $K$ are the same with respect to $x_{conv}$[1]. Each case was accelerated until its transition was completed. This resulted in the temporal acceleration having a higher final Reynolds number to accommodate the later transition in this flow (see figure 2c). In this study, an initial Reynolds number, $Re_b = U_b\delta/\nu$ of 2800 is used, where $\delta$ is the half-channel height. The details of the cases are shown in table 1. The bulk velocity profiles for the moving wall (case M) and temporal (case T) accelerations are shown in figure 2. Figure 2c confirms the equivalence between

[1]For the moving-wall acceleration, $K = \frac{1}{Re \cdot U_b^2}\frac{dU_b}{dx}$. For the temporal acceleration, $K = \frac{1}{Re \cdot U_b^3}\frac{dU_b}{dt}$

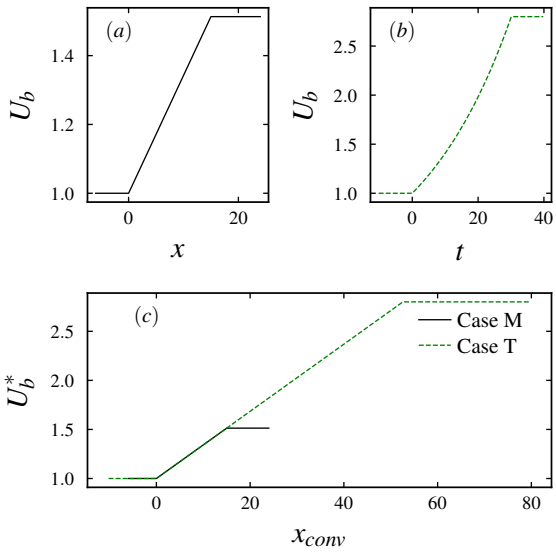


Figure 2. $(a)$ Relative bulk velocity for case M. $(b)$ Bulk velocity for case T. $(c)$ Comparison of case M and T with case T plotted against convective distance.

the bulk velocity profile in cases M and T when plotted against convective distance. The statistics for case M have been averaged in the spanwise direction, and at many times. Case T has been averaged in the spanwise and streamwise directions, and ensemble-averaged using six independent simulations. Unless otherwise stated, the velocity is normalised by the initial bulk velocity, $U_{b0}$, the distance by the half-channel height, $\delta$, and time by $\delta/U_{b0}$.

## RESULTS AND DISCUSSION

Figure 3 presents the instantaneous streamwise and wall-normal velocity fluctuations for case M. Figure 3a shows that the near-wall streaks mildly strengthen from the onset of the acceleration ($x = 0$) while $v'$ (figure 3b) does not initially respond. The strengthening of the streaks is linked to the stretching of the near-wall turbulent structures by the mean shear associated with the development of the new boundary layer that forms with the onset of the acceleration. At $x \approx 8$, coincident spots can be observed in $u'$ and $v'$ that are initially localised in space but grow as they are convected downstream until the entire surface of the wall is covered in new turbulence structures. Figure 4 presents $u'$ and $v'$ for case T at a time around the onset of transition showing the strengthened and elongated streaks coexisting with the localised turbulent spots. These results are consistent with previous studies of the moving-wall and temporal acceleration, which have split the flow development into three regions: Pre-transition ($0 < x \leq 8$), the initial phase characterised by the strengthening of near-wall streaks; transition ($8 < x \leq 14$), the phase characterised by the forma-

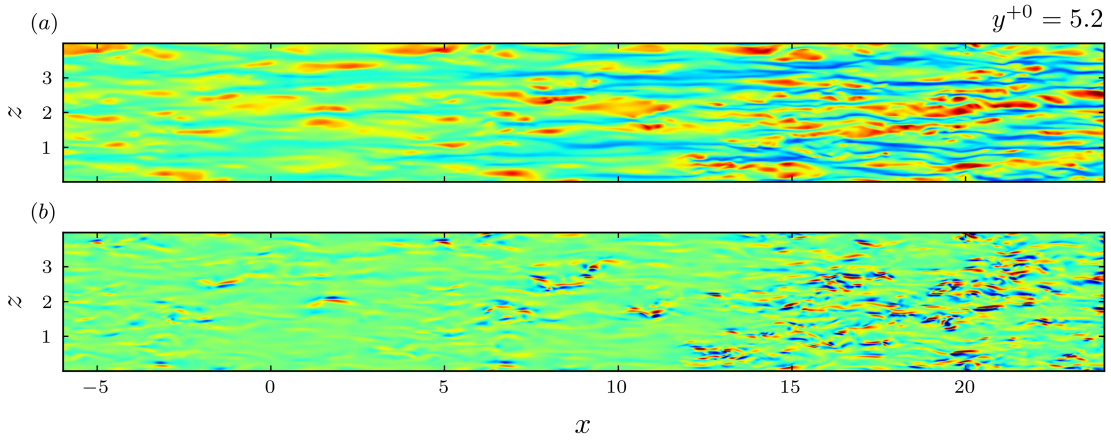


Figure 3. Contours of fluctuating velocity for case M at $y^{+0} = 5.2$. $(a)$ $u'$. $(b)$ $v'$

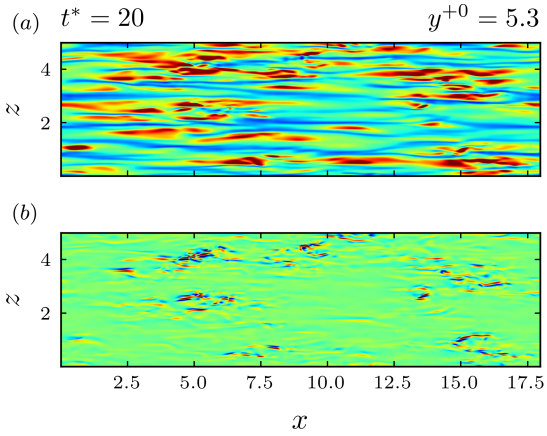


Figure 4. Contours of fluctuating velocity for case T at a time near the onset of transition ($t^* = 20$) showing the presence of turbulent spots. $(a)$ $u'$. $(b)$ $v'$.

tion and growth of turbulent spots; and fully turbulent ($x > 14$), the region after the merging of the near-wall turbulent spots which is largely characterised by the wall-normal diffusion of the newly generated turbulence.

The flow characteristics can also be understood through the second-order statistics, which are shown in figure 5 with locations before the onset of transition coloured blue and those after coloured red. The strengthening of the near-wall streaks during pre-transition in both cases M and T is indicated by the increases in $\overline{u'u'}$ (figures 5$(a,e)$). The initial lack of response from the other turbulent components can be seen in figure 5$(b,f)$, which shows $\overline{v'v'}$. These figures also show the sudden change in the behaviour of $\overline{v'v'}$ with the onset of transition with growth occurring over a large wall-normal region, particularly for the case T, which grows by nearly an order of magnitude. The growth of the $-\overline{u'v'}$ (figures 5$(c,g)$) in both cases is also similar, with increases during pre-transition being limited to the near-wall region with broad increases during the transition phase. The eddy viscosity, which can be considered an indicator of turbulence activities, is presented in figures 5$(d,h)$. During pre-transition, there is no change to this quantity, indicating that the fundamental turbulence characteristics of flow remain largely unchanged and that the increases observed $\overline{u'v'}$ are related to increases in mean shear. This is consistent with previous studies of accelerating channel flows (Falcone & He, 2022; He & Seddighi, 2013).

## Skin friction coefficient and FIK Identity

While figures 3 to 5 show that qualitatively the flows develop in a remarkably similar fashion, differences emerge when the accelerations are compared against convective distance. Figure 6 shows the skin friction coefficient, $C_f$ and its FIK identity (Fukagata *et al.*, 2002), which is defined as

$$C_f = \underbrace{\frac{6}{Re_b}}_{C_f^L} \underbrace{-6\int_0^1 (1-y)(\overline{u'v'})dy}_{C_f^T} \underbrace{-3\int_0^1 (1-y)^2\left(I+\frac{\partial p''}{\partial x}\right)dy}_{C_f^I}. \quad (4)$$

The behaviour of $C_f$ is generally similar in both cases, with an initial increase before decreasing to a minimum and thereafter increasing. For accelerating flows, the minimum in the skin friction coefficient is considered an approximate marker for the onset of transition (He & Seddighi, 2013), and it can be seen that the convective distance where the minimum occurs is substantially delayed in case T compared with case M. It should also be noted that the initial increases in $C_f$ are very weak in case M. The FIK decomposition reveals that these differences can be associated with inertial contribution, $C_f^I$, which exhibits significant increases in case T but remains limited in case M. The differences in the development of the inertia terms between the temporal and moving-wall acceleration are explored below.

## Momentum balance and pseudo body force approach

In order to better understand the differences between the accelerations, we can analyse the streamwise mean momentum equations which are given below for the temporal (equation 5) and moving-wall acceleration (equation 6) with only the dominant right-hand side terms shown.

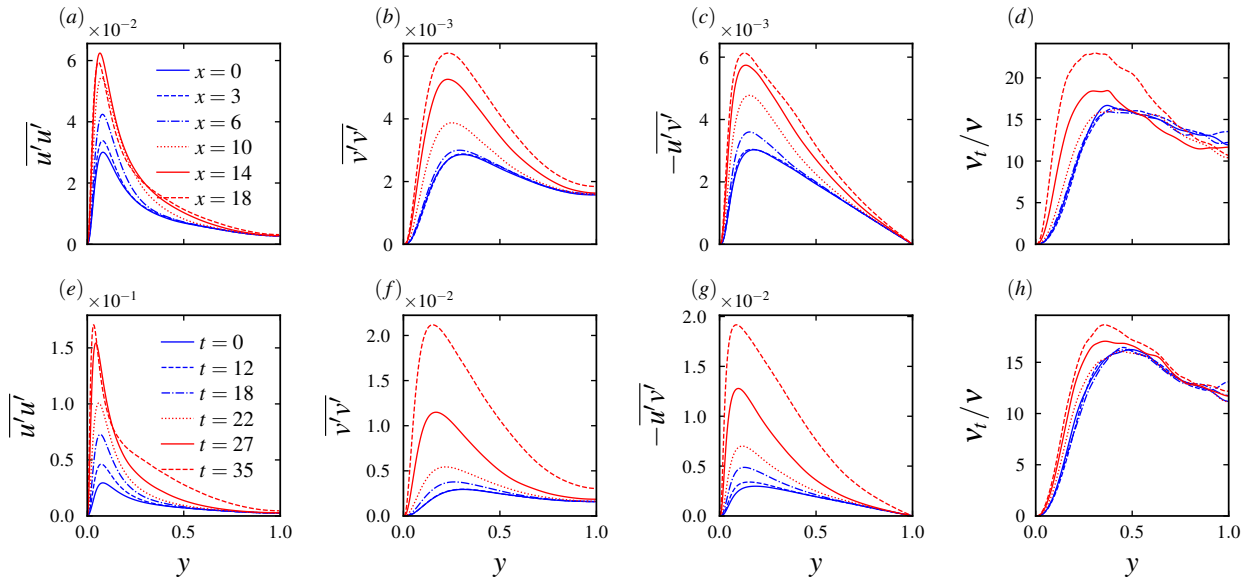


Figure 5. Second-order statistics. $(a,e)$ $\overline{u'u'}$, $(b,f)$ $\overline{v'v'}$, $(c,g)$ $\overline{u'v'}$, $(d,h)$ $\nu_t$. Case M is shown in $(a,b,c,d)$ and case T is shown in $(e,f,g,h)$. Locations or times before the onset of transition are shown in blue and those after in red for clarity. The streamwise locations for case M are located in $(a)$ and the times for case T are located in $(e)$.

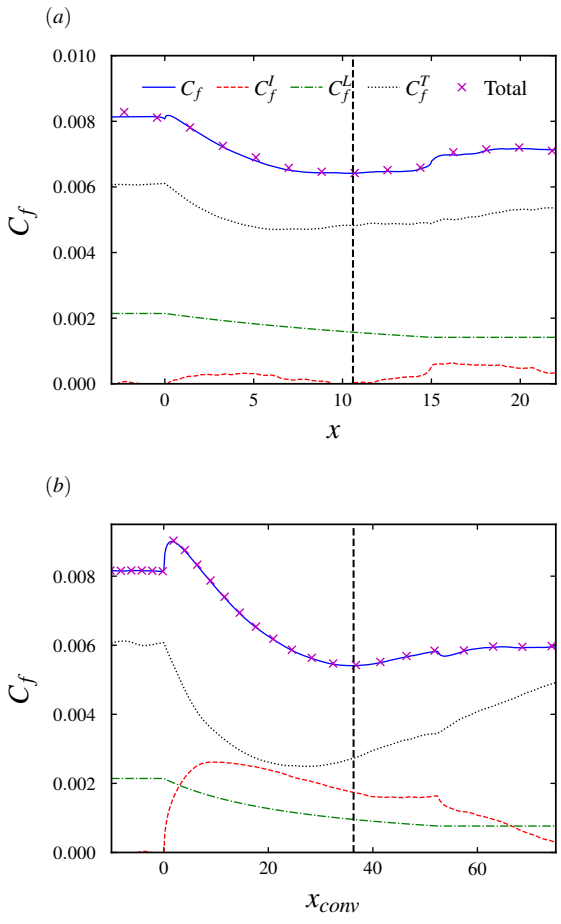


Figure 6. Skin friction coefficient and FIK identity for cases M $(a)$ and T $(b)$. Vertical line indicates the minimum in $C_f$ for each case.

$$\underbrace{\frac{\partial \bar{u}}{\partial t}}_{-f_T} = -\frac{\partial \bar{p}}{\partial x} + \frac{\partial}{\partial y}\left(\frac{1}{Re}\frac{\partial \bar{u}}{\partial y} - \overline{u'v'}\right) \tag{5}$$

$$\bar{u}\frac{\partial \bar{u}}{\partial x} + \bar{v}\frac{\partial \bar{u}}{\partial y} = -\frac{\partial \bar{p}}{\partial x} + \frac{\partial}{\partial y}\left(\frac{1}{Re}\frac{\partial \bar{u}}{\partial y} - \overline{u'v'}\right). \tag{6}$$

The development of the moving wall acceleration can be better understood as a relative acceleration using the substitution $\bar{u} = \bar{u}_{rel} - U_w$ in equation 6, which results in modified convection terms:

$$\underbrace{\bar{u}_{rel}\frac{\partial \bar{u}_{rel}}{\partial x}}_{-f_A} + \underbrace{\bar{u}_{rel}\frac{\partial U_w}{\partial x} + U_w\frac{\partial \bar{u}_{rel}}{\partial x}}_{-f_B} + \underbrace{U_w\frac{\partial U_w}{\partial x}}_{-f_C} + \underbrace{\bar{v}\frac{\partial \bar{u}_{rel}}{\partial y}}_{-f_D} = RHS. \tag{7}$$

Equation 1 was determined to equate the bulk temporal inertia with the bulk relative acceleration of the moving wall acceleration. As a result, term $f_A$ can be considered broadly comparable with $f_T$ in equation 5. The substitution also results in the additional terms $f_B$ and $f_C$, as well as term $f_D$, which is unchanged by the substitution. The effect of these terms on the flow response needs to be determined, particularly in the pre-transition region.

The theory that has been developed for the temporal and moving-wall accelerations considers the flow development to be characterised by the formation and development of a new boundary layer superimposed on the pre-existing turbulent flow. As a result, the flow development can be considered with the following decomposition:

$$\bar{u} = \bar{u}_0 + \bar{u}^{\wedge}, \tag{8}$$

where $\bar{u}_0$ is the pre-existing flow and $\bar{u}^\wedge$ is a perturbation flow, which results from the imposition of the acceleration and incorporates the new boundary layer. We can consider the terms on the left-hand side of equations 7 and 5 as *pseudo-body forces* and moved to the right-hand side of the equation with the resulting equations for the pre-existing flow and the flow after the onset of the acceleration given as

$$0 = -\frac{\partial \bar{p}_0}{\partial x} + \frac{\partial}{\partial y}\left(\frac{1}{Re}\frac{\partial \bar{u}_0}{\partial y} - \overline{u'v'}_0\right), \tag{9}$$

$$0 = -\frac{\partial \bar{p}}{\partial x} + \frac{\partial}{\partial y}\left(\frac{1}{Re}\frac{\partial \bar{u}}{\partial y} - \overline{u'v'}\right) + f. \tag{10}$$

For the case T, $f = f_T$ and for case M, $f = f_A + f_B + f_C + f_D$. An equation for the perturbation flow, $\bar{u}^\wedge$ can be developed by subtracting equation 9 from equation 10.

$$0 = -\frac{\partial \bar{p}^\wedge}{\partial x} + \frac{\partial}{\partial y}\left(\frac{1}{Re}\frac{\partial \bar{u}^\wedge}{\partial y} - \overline{u'v'}^\wedge\right) + f, \tag{11}$$

where $\overline{u'v'}^\wedge = \overline{u'v'} - \overline{u'v'}_0$. During the pre-transition region, figure 5$(d,h)$ shows that the eddy viscosity, $\nu_t$ remains unchanged from the pre-existing flow hence $\nu_t = \nu_{t0}$. Also note that $\nu_{t0}$ is the same for case T and case M as their pre-existing flows are the same. Invoking the Boussinesq hypothesis and considering the dominant strain rate only,

$$\overline{u'v'}^\wedge = \frac{\nu_{t0}}{Re}\left(\frac{\partial \bar{u}}{\partial y} - \frac{\partial \bar{u}_0}{\partial y}\right) = \frac{\nu_{t0}}{Re}\frac{\partial \bar{u}^\wedge}{\partial y}. \tag{12}$$

Substituting equation 12 into equation 10 results in

$$0 = -\frac{\partial \bar{p}^\wedge}{\partial x} + \frac{\partial}{\partial y}\left(\frac{1+\nu_{t0}}{Re}\frac{\partial \bar{u}^\wedge}{\partial y}\right) + f. \tag{13}$$

The perturbation pressure gradient, $\frac{\partial \bar{p}^\wedge}{\partial x}$ can be eliminated by considering the following assumptions (these can be confirmed by analysing momentum equation balance for cases M and T):

1. The pressure gradient is constant across the wall-normal extent of the channel.
2. The flow development during pre-transition is limited to the near-wall region and hence $\frac{\partial \bar{u}^\wedge}{\partial y} = 0$ around the channel centreline.

Hence, taking the force balance at the channel centreline results in

$$\frac{\partial \bar{p}^\wedge}{\partial x} = f_U, \tag{14}$$

where $f_U$ is the body force at the centreline, which is hereafter referred to as the uniform body force with the non-uniform component defined as $f_N = f - f_U$. Substituting equation 14 into equation 13 results in an equation for the perturbation flow associated with acceleration in terms of the non-uniform inertia pseudo-body forces:

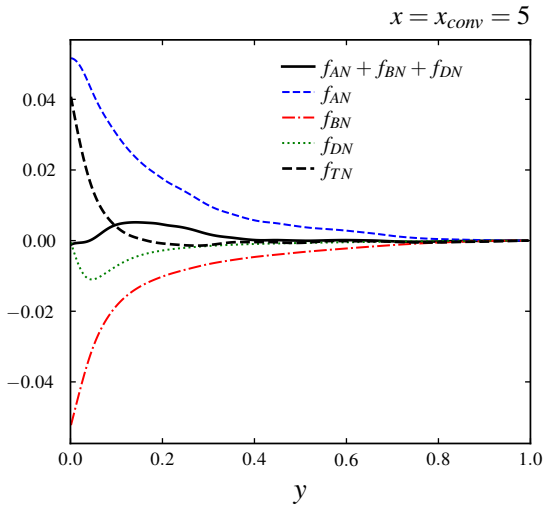


Figure 7. Non-uniform body forces for cases T and case M at $x_{conv} = 5$

$$0 = -\frac{\partial}{\partial y}\left(\frac{1+\nu_{t0}}{Re}\frac{\partial \bar{u}^\wedge}{\partial y}\right) + f_{TN}. \tag{15}$$

$$0 = \frac{\partial}{\partial y}\left(\frac{1+\nu_{t0}}{Re}\frac{\partial \bar{u}^\wedge}{\partial y}\right) + f_{AN} + f_{BN} + f_{DN}, \tag{16}$$

with $f_{CN} = 0$. The profiles of these body forces at $x_{conv} = 5$ for cases T and M are given in figure 7, which shows that $f_{AN}$ has a similar overall profile to $f_{TN}$, although its magnitude is significantly larger. Body forces $f_{BN}$ and $f_{DN}$ are significant and oppose $f_{AN}$, which results in the total non-uniform body force being a significantly different shape to $f_{TN}$ particularly close to the wall. This different near-wall behaviour of the body forces helps to explain why there is a much more limited increase in skin friction coefficient for case M. Further understanding of the effect of these differences on the transition process will be an aspect of future work with an emphasis on comprehensively understanding the substantially earlier transition in the moving-wall acceleration.

## CONCLUSION

- A comparison of a temporal and an idealised spatial acceleration using moving walls has been conducted such that the bulk velocities are the same with respect to a convective distance. This was achieved by equating the bulk temporal inertia with the relative bulk inertia of the moving wall acceleration
- The behaviours of the two flows are qualitatively similar to each other, as shown through the Reynolds stresses and instantaneous results. These results were also found to conform to the transition theory developed from He & Seddighi (2013).

- Despite the similarities, the detailed flow development contains a number of significant differences, particularly in the response of the skin friction coefficient in the early stages of the acceleration, where the increases in $C_f$ in moving-wall acceleration are much more limited. It was also found that the point of transition occurred substantially earlier in the moving wall case.
- The convection terms of the momentum equation for the moving wall acceleration were decomposed to consider the relative flow acceleration. This resulted in additional terms which were analysed using a pseudo-body force approach similar to He *et al.* (2021). This showed that the convection in the moving-wall acceleration behaves in a significantly different manner to the temporal acceleration, which may be used to explain the quantitative differences in the turbulence response in the two flows.

## Acknowledgements

This work makes use of the DNS code CHAPSim, which is currently maintained by CCP-NTH (EP/T026685/1). High performance computing resources on ARCHER2 were provided by the UK Turbulence Consortium (EP/R029326/1).

## REFERENCES

Coleman, Gary N, Kim, John & Le, Anh-Tuan 1996 A numerical study of three-dimensional wall-bounded flows. *International Journal of Heat and Fluid Flow* **16**, 333–342.

Falcone, M. & He, S. 2022 A spatially accelerating turbulent flow with longitudinally contracting walls. *Journal of Fluid Mechanics (submitted)* .

Fukagata, Koji, Iwamoto, Kaoru & Kasagi, Nobuhide 2002 Contribution of reynolds stress distribution to the skin friction in wall-bounded flows. *Physics of Fluids* **14**, L73–L76.

Guerrero, Byron, Lambert, Martin F. & Chin, Rey C. 2021 Transient dynamics of accelerating turbulent pipe flow. *Journal of Fluid Mechanics* **917**, A43.

He, J., Tian, R., Jiang, P.X. & He, S. 2021 Turbulence in a heated pipe at supercritical pressure. *Journal of Fluid Mechanics* **920**, 45.

He, S. & Seddighi, M. 2013 Turbulence in transient channel flow. *Journal of Fluid Mechanics* **715**, 60–102.

Kozul, M., Chung, D. & Monty, J. P. 2016 Direct numerical simulation of the incompressible temporally developing turbulent boundary layer. *Journal of Fluid Mechanics* **796**, 437–472.

Seddighi-Moormani, Mehdi 2011 Study of turbulence and wall shear stress in unsteady flow over smooth and rough wall surfaces.

Sundstrom, L. R. Joel & Cervantes, Michel J. 2018 The self-similarity of wall-bounded temporally accelerating turbulent flows. *Journal of Turbulence* **19**, 49–60.

Wray, A. & Hussaini, M. Y. 1984 Numerical experiments in boundary-layer stability. *Proceedings of the Royal Society of London. A. Mathematical and Physical Sciences* **392**, 373–389.